NANO LETTERS

pubs.acs.org/NanoLett

Letter

Directional Emission from Electrically Injected Exciton−Polaritons in Perovskite Metasurfaces

Yutao Wang, Jingyi Tian, Maciej Klein, Giorgio Adamo, Son Tung Ha,* and Cesare Soci*

Cite This: *Nano Lett.* 2023, 23, 4431−4438

Read Online

ACCESS | Metrics & More | Article Recommendations | Supporting Information

ABSTRACT: We present a new approach to achieving strong coupling between electrically injected excitons and photonic bound states in the continuum of a dielectric metasurface. Here a high-finesse metasurface cavity is monolithically patterned in the channel of a perovskite light-emitting transistor to induce a large Rabi splitting of ∼200 meV and more than 50-fold enhancement of the polaritonic emission compared to the intrinsic excitonic emission of the perovskite film. Moreover, the directionality of polaritonic electroluminescence can be dynamically tuned by varying the source-drain bias, which induces an asymmetric distribution of exciton population within the transistor channel. We argue that this approach provides a new platform to study strong light−matter interactions in dispersion engineered photonic cavities under electrical injection and paves the way to solution-processed electrically pumped polariton lasers.

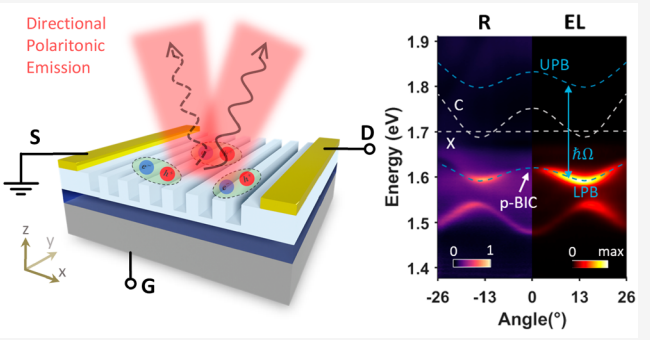

KEYWORDS: *metal halide perovskites, electrically injected exciton−polaritons, dielectric metasurfaces, bound states in the continuum, light-emitting transistor, strong coupling*

Exciton−polaritons are bosonic quasiparticles arising from strong coupling between excitons and confined photons. The hybrid nature equips exciton−polaritons with extremely small effective mass, strong nonlinearities and fast relaxation,[1,2] properties that make them a unique platform for fundamental studies such as Bose−Einstein condensation and superfluidity, as well as for the realization of optoelectronic devices such as quantum simulators, neuromorphic computing and inversionless lasers.[3−12] While electrically injected polaritons could enable the realization of electrically pumped polariton lasers, polariton circuits, and high-speed communication systems, so far polaritonic devices have mostly been driven by optical excitation.

The typical platform for studying electrically driven exciton−polaritons is that of light-emitting diodes (LEDs) integrated with distributed Bragg reflector (DBR) microcavities,[13−15] which has inherent limitations to further manipulation of the polaritonic emission. Dielectric metasurfaces, on the other hand, enable complete mode and dispersion engineering of the polaritons, but achieving electrically driven exciton−polaritons in metasurfaces is challenging due to the need for smooth contacts between the active materials and the charge injection layers to guarantee efficient charge carrier transport. By comparison, the lateral configuration of light-emitting transistor (LET) devices enables the fabrication of metasurfaces directly in the emission zone, with minimal degradation of device performance.[16] This provides the opportunity to design metasurfaces that support high *Q*-factor modes such as bound states in the continuum (BICs), which could ensure strong confinement of photonic modes in the active layer and lead to stronger light−matter interactions under electrical excitation. The lateral configuration of the LET also allows inducing an unbalanced charge carrier distribution within the active metasurface by adjusting the source-drain bias, which could be used to tune the directionality of the polaritonic emission.

In this work, we demonstrate electrically driven exciton−polaritons in a perovskite LET with metasurfaces directly patterned into the open surface between the top electrodes. Metal halide perovskites are chosen as both active medium and dielectric matrix due to their unique combination of high optical gain and luminescence quantum yield, good charge carrier transport, and high refractive index.[17−20] Importantly, excitons in perovskite can possess large binding energy, strong nonlinearities, and large oscillator strength, which highly benefit the study of exciton−polaritons.[21−28] We observe the formation of high-quality factor polariton BICs (p-BICs) due to the strong coupling between the photonic BICs supported

Received: February 24, 2023
Revised: April 23, 2023
Published: May 2, 2023

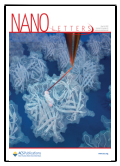

https://doi.org/10.1021/acs.nanolett.3c00727
Nano Lett. 2023, 23, 4431−4438

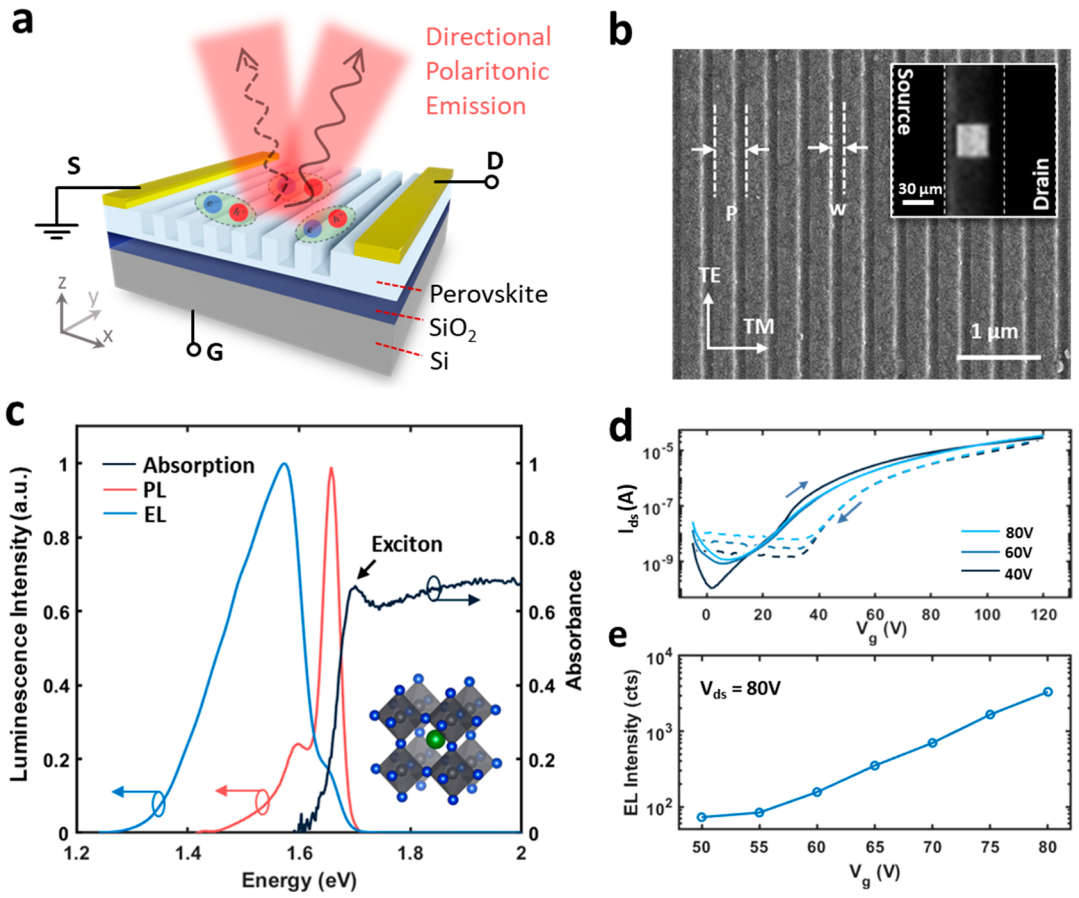

Figure 1. Electrically driven polaritonic perovskite metadevice. (a) Schematic of the electrically driven perovskite metasurface with tunable polaritonic emission. A resonant dielectric metasurface is monolithically fabricated within the active region of the transistor between the source (S) and drain (D) electrodes, leading to strong coupling of photonic modes and electrically injected excitons. The resulting polaritonic EL intensity and directionality can be controlled by the gate (G) and source-drain biases, respectively. (b) SEM image of the perovskite nanobeam array fabricated by FIB lithography within the active region between the top S-D electrodes. The perovskite nanobeams had a period (P) ranging from 380 and 400 nm, a height of 125 nm, and a spacing (w) of 100 nm. The optical microscope image of the device operating at $V_g = \pm 80$ V and $V_{ds} = 80$ V in the inset shows the region of enhanced EL corresponding to the nanopatterned region of the square metasurface. (c) PL and absorption spectra of the $MAPbI_3$ perovskite compared to the EL spectrum of the unpatterned LET at 78 K. The crystal structure of the $MAPbI_3$ perovskite is shown in the inset, where green, black, and blue spheres represent MA^+, Pb^{2+} and I^- ions, respectively. (d) Transfer characteristics of the $MAPbI_3$ LET obtained in the forward and backward sweeping direction of gate bias with $V_{ds} = 40$, 60, and 80 V. (e) Peak EL intensity dependence on AC gate bias with $V_{ds} = 80$ V.

by the metasurface and the perovskite excitonic resonance, leading to a Rabi splitting energy of ~200 meV and more than 50-fold enhancement of the electroluminescence (EL) from the lower polariton band (LPB) over the intrinsic excitonic emission. Furthermore, we show that the directionality of the polaritonic emission can be dynamically tuned through group velocity selection under reversed electrical biases. Overall, these results build a foundation for a new class of electrically driven light-emitting polaritonic devices empowered by functional designer metasurfaces, which could enable new fundamental discoveries and practical applications such as electrically driven polariton lasers and tunable perovskite polaritonic devices.

The high refractive index of metal halide perovskites allows the monolithic integration of functional dielectric metasurfaces in light-emitting devices.[16,20,29−32] Here LETs with lateral electrode configurations are employed for the accessibility of their active region to metasurface nanofabrication (Figure 1). Methylammonium lead iodide ($MAPbI_3$) LETs were fabricated as detailed in the "Materials and Methods" section of the Supporting Information and elsewhere.[33−35] The transistor has a top-contact, bottom-gate configuration, with gold (Au) and p-doped Si as the source-drain electrodes and gate electrode, respectively (Figure 1a). To create the monolithic light emitting metadevice, the metasurface is directly patterned by focused ion beam (FIB) lithography (Figure 1b). The metasurface, consisting of periodic nanobeams oriented parallel to the Au electrodes, serves as an optical cavity that supports photonic resonances. The highly confined cavity photons can strongly couple with excitons generated or injected in $MAPbI_3$ to form exciton−polaritons. The inset of Figure 1b shows a microscope image of the operating LET in which the bright square in the middle of the electrodes corresponds to EL emission from the metasurface area. Figure 1c shows the low-temperature absorption and photoluminescence (PL) properties of $MAPbI_3$, where the absorption peak at 1.70 eV corresponds to the excitonic resonance of the perovskite, while the PL displays a dominant peak at ~1.66 eV and a minor peak at 1.60 eV, which can be attributed to the orthorhombic and tetragonal phases of $MAPbI_3$, respectively.[36]

https://doi.org/10.1021/acs.nanolett.3c00727
Nano Lett. 2023, 23, 4431−4438

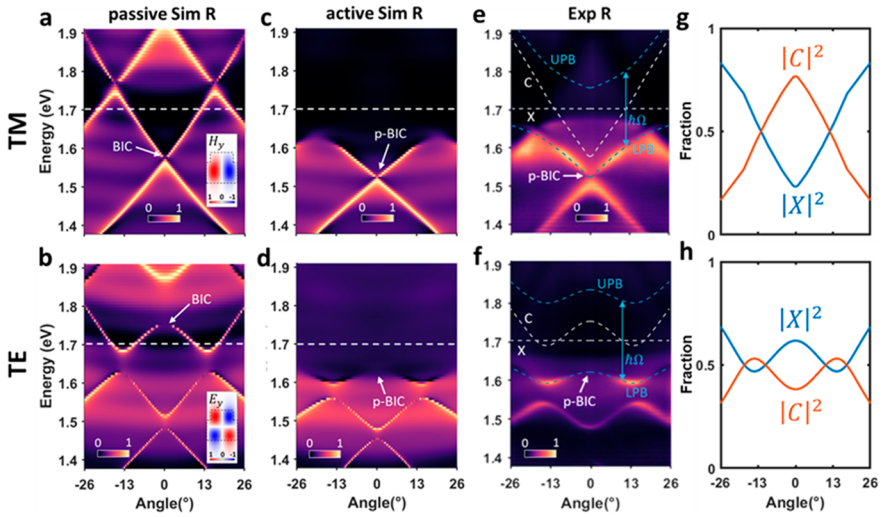

Figure 2. Strong coupling of photonic BICs and perovskite excitonic resonances. (a, b) Calculated angle-resolved reflection spectra for TM (a) and TE (b) polarized illumination of the passive perovskite metasurface (i.e., assuming zero absorption and a fixed refractive index n = 2.4). The white dashed lines indicate the position of the excitonic resonance of $MAPbI_3$ at ∼1.70 eV. The insets show the field distribution in the $x-z$ plane of the TM and TE polarized BICs. (c, d) The simulated angle-resolved spectra of the active perovskite metasurface (P = 400 nm) with TE and TM polarizations. (e, f) Experimental angle-dependent reflection spectra of the active perovskite metasurface under TM and TE illumination, respectively. The white dashed lines indicate the band structure of the passive metasurface (C) and the excitonic resonance (X) of $MAPbI_3$. The blue dashed lines represent the theoretically fitted LPBs and the UPBs. The polariton BICs are indicated by white arrows. (g, h) Hopfield coefficients of the corresponding polaritons, showing exciton and photon fractions in the LPBs for TM and TE polarizations, respectively.

To increase brightness and uniformity of the EL, the device is operated under an alternating current (AC) gate voltage (V_g) of ±80 V and a constant source-drain voltage (V_{ds}) of 80 V. Note that the relatively large bias voltages needed to operate the LETs are due to the large channel length and may be substantially reduced by decreasing the electrode gap or increasing the gate capacitance (e.g., adopting thinner SiO_2 layers or high-k dielectric materials).[37] The EL spectrum of the unstructured LETs peaks at 1.58 eV. The red-shifted and broadened EL spectrum compared to the PL may be attributed to self-absorption and re-emission of the EL that originates within the transistor channel, that is, at the perovskite/substrate interface, compared to the PL that is primarily emitted from the top surface of the perovskite film.[38,39] The gate bias dependence of the LET transport and EL characteristics is shown in Figure 1d,e. The perovskite LET transfer characteristics show predominantly n-type charge transport behavior with an on−off ratio larger than 10^3 and electron mobilities up to ∼0.16 $cm^2V^{-1}s^{-1}$ (Figure 1d). The EL intensity is found to increase nearly exponentially when the gate voltage increases from 50 to 80 V (Figure 1e). The strong dependence of the EL intensity on gate bias confirms that the device operates in the enhancement regime.

To fulfill the criteria of strong coupling, the averaged decay rate of the excitonic (γ) and photonic resonances (κ) has to be smaller than the rate of the energy exchange (g) between them, i.e., $2g \geq (\kappa + \gamma)/2$.[21] Since κ is inversely proportional to the quality factor (Q) of the photonic cavity, a high Q cavity eases the strong coupling requirement. Here, we adopt a nanobeam metasurface that supports photonic BICs with extremely high radiative Q-factor to facilitate the formation of exciton−polaritons (Figure 2). To understand the formation of BICs in the nanobeam structures, we simulated the photonic bands of the passive cavity (i.e., the perovskite replaced by a dielectric medium with a fixed refractive index n = 2.4) with P = 400 nm for TM and TE polarization, as shown in Figure 2a,b, respectively. Both TM and TE polarizations support symmetry-protected BICs at the Γ-point located near 1.58 and 1.76 eV, respectively, indicated by the white arrow. The BICs are evidenced by the vanishing reflectance at the normal incidence, corresponding to the intrinsic near-zero line width and the ultrahigh radiative Q-factor of the passive metasurface (Figure S1). The field distribution of the symmetry-protected BICs is shown in the insets, providing a visual clue that the BICs can hardly couple to the vertical plane wave due to symmetry mismatch.[40]

Angle-resolved reflection measurements are used to validate the coupling between the perovskite exciton resonances and the photonic BICs in the perovskite metasurface. The experiments were conducted at cryogenic temperature (i.e., T = 78 K) using a home-built microspectrometer setup with back-focal plane (BFP) capability[41] (details on the experimental setup are provided in Figure S2). The measured reflection spectra under TM and TE polarization excitation shown in Figure 2e,f are in excellent agreement with the simulated reflection band structures of the active metasurface (Figure 2c,d) calculated by taking into account the dispersion of the refractive index at T = 78 K (Figure S3).[19] Anticrossing behavior between the photonic (C) and excitonic (X) bands can be observed for both TM and TE polarizations, a clear signature of strong coupling. A coupled oscillator model was used to calculate upper (UPB) and lower polariton branches (LPB),[2] showing good agreement with the reflection measurement results (see details of the model in Supporting Information). Under cavity detuning of Δ_{TM} = −126 meV (Δ_{TE} = 53 meV), the Rabi splitting energy is estimated to be 202 meV (206 meV) for the TM mode (TE mode). This is much larger than the averaged damping rates of the excitonic and photonic resonances (39 meV, as derived from the averaged line width), confirming the system is able to reach the strong coupling regime. Note that the upper polariton bands can hardly be distinguished in the experiment due to strong

https://doi.org/10.1021/acs.nanolett.3c00727
Nano Lett. 2023, 23, 4431−4438

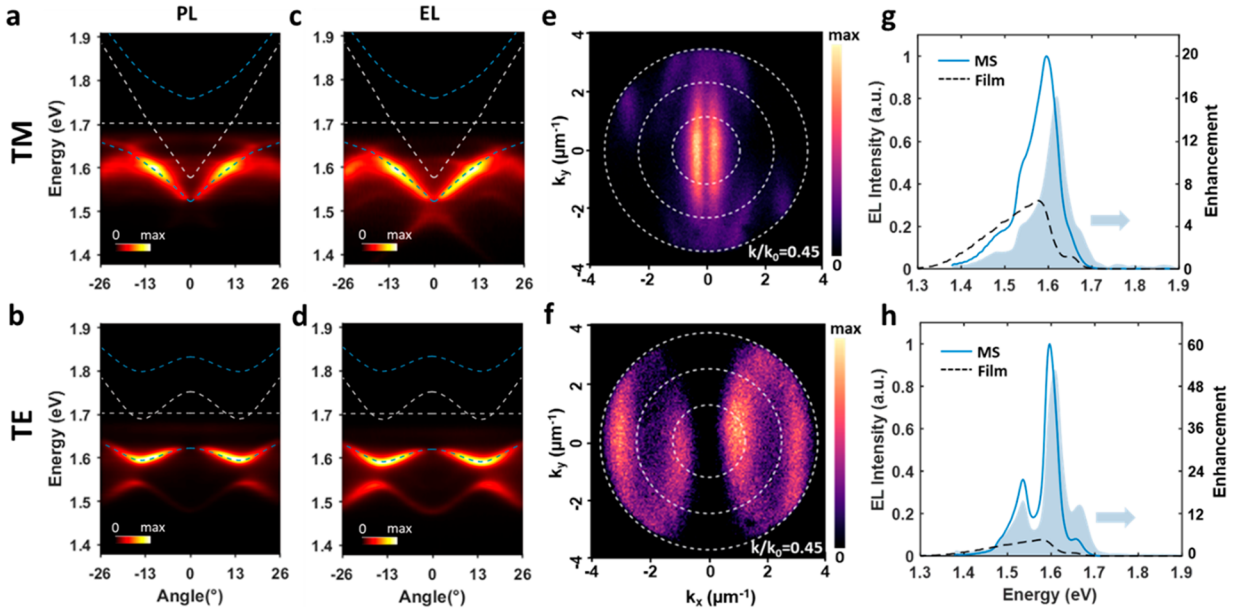

Figure 3. Polaritonic emission from perovskite metasurface. (a, b) Angle-resolved PL spectra of the perovskite metasurface. (c, d) Angle-resolved EL spectra of the perovskite metasurface in the LET operating under V_{ds} = 80 V, V_g = ± 80 V. (e, f) k-space far-field profiles of the p-BICs, obtained with a 10 nm band-pass filter centered at 810 nm (1.53 eV) for TM and 760 nm (1.63 eV) for TE polarization. The white dashed circles, from the inner to the outer, indicate the numerical aperture (NA) of 0.15, 0.3, and 0.45. (g, h) EL intensity of the perovskite metasurface (blue line) and the perovskite film (black dashed line), along with the EL enhancement (blue shaded area) obtained as the ratio of the two.

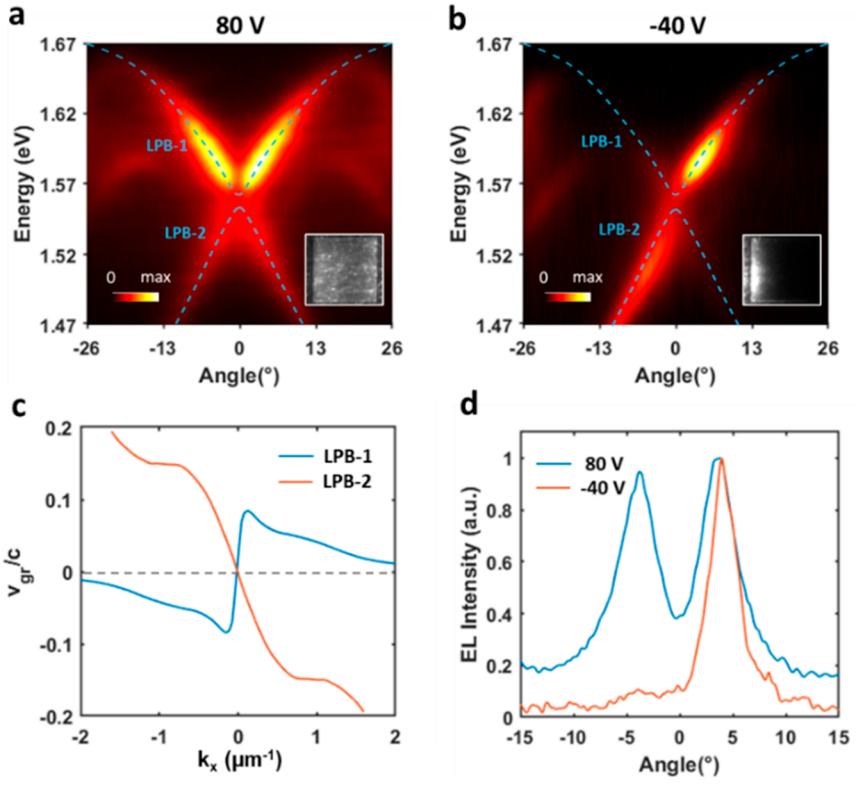

Figure 4. Electrically tunable directional polaritonic emission. TM polarized angle-resolved EL spectra of the perovskite metasurface with P = 380 nm, V_g = ± 80 V and (a) V_{ds} = 80 V or (b) V_{ds} = −40 V. Fitting of the LPB-1 and LPB-2 are indicated by the blue dashed lines. The insets show optical microscope images of the corresponding metasurface area (30 μm × 30 μm). (c) Normalized polariton group velocity of the LPB-1 and LPB-2 extracted from the dispersion in a). (d) Directional EL of LPB-1 at the energy of 1.57 eV obtained by applying 80 V (blue line) and −40 V (orange line) source-drain voltage.

absorption above the exciton energy.[22,42] The Hopfield coefficients of the system, representing the fraction of the excitons ($|X|^2$) and the photons ($|C|^2$) in the LPBs for TM and TE polarizations, are calculated by the coupled oscillator

https://doi.org/10.1021/acs.nanolett.3c00727
Nano Lett. 2023, 23, 4431−4438

model and are shown in Figure 3g,h, respectively. Photons and excitons are equally mixed in the polariton branches at the angle where the passive photonic bands cross the excitonic resonance. In our case, at the Γ-point, the TM (TE) polarized polariton branch has an exciton fraction of 23% (62%), indicating the hybrid nature of the polariton BICs. The significant excitonic fractions of TE and TM polaritons in their LPBs are expected to facilitate polariton relaxation into lower energy states, which may eventually lead to condensation and inversionless lasing.[1,12,43,44]

Strong coupling of photonic BICs and excitonic resonances is also manifested by the polaritonic character of PL and EL properties of the perovskite metasurface (Figure 3). Angle-resolved PL spectra of the perovskite nanobeam array excited by an off-resonance laser show a clear enhancement of the emissions from the LPBs, in good agreement with the theoretical predictions for both TM and TE polarizations (Figure 3a,b). To demonstrate electrically driven exciton−polaritons in the perovskite metasurface, the device was operated under an AC gate voltage, and the angle-resolved EL spectra were recorded for TM and TE polarizations (Figure 3c,d). Like PL, the EL spectra also show clear enhancement of polaritonic emission from the LPBs, confirming the generation of exciton−polaritons under electrical injection. It is worth noting that the outcoupling of the p-BICs at 1.53 eV for TM polarization (1.62 eV for TE polarization) to the radiative continuum is strictly forbidden due to the intrinsic symmetry mismatch inherited from the photonic BICs. The p-BIC nature of the modes is confirmed by the decrease in intensity, the reduction in line width and the increase of the *Q*-factor near the normal emission direction, as seen in Figure S4. The dispersion of the polaritonic bands with bright modes at the Γ-point for both polarizations is also shown in Figure S5 based on the same analysis procedure.

The far-field profile of the electrically driven p-BICs was analyzed in the *xy*-reciprocal space. Figure 3e,f shows the BFP image of the p-BICs around 1.53 eV (1.63 eV) for TM (TE) polarization. The EL at the normal direction ($k_x = 0$) is found to vanish even at large k_y for both polarizations, matching well the simulated profile (Figure S6). Interestingly, the polaritonic EL reaches a maximum 56-fold enhancement at 1.607 eV under TE polarization and 15-fold enhancement at 1.620 eV under TM polarization compared to the excitonic emission from the unstructured portions of the device channel due to Purcell enhancement and scattering from the exciton reservoir into the LPB (Figure 3g, h).[45] The integrated enhancement is calculated to be 4.8-fold and 1.9-fold for TE and TM polarizations, respectively. Overall, the monolithically structured metasurface yields higher emission directionality and higher density of states in the LPBs, thanks to the strong coupling. As discussed in the following, we believe that these characteristics provide new opportunities to realize highly efficient and tunable polaritonic devices and, potentially, electrically driven polariton lasers.

Unlike conventional LEDs where charge injection, and thus emission, is homogeneous across the active region of the device in the vertical multilayer stack, the charge carrier distribution in the channel of LETs can be controlled by adjusting the source-drain bias.[35,46] This characteristic feature of the LETs was exploited to prove the reversible tunability of the directionality of the exciton−polariton EL (Figure 4). Figure 4a shows the angle-resolved EL spectra of the nanostructured perovskite LET with detuning energy Δ_{TM} = −73.1 meV (P = 380 nm) with V_{ds} = 80 V, which induces uniform EL emission throughout the metasurface area (inset of Figure 4a). At these biasing conditions, two symmetric LPBs (LPB-1 and LPB-2) can be observed in the EL spectrum. Note that the enhanced polariton relaxation in LPB-1, characterized by the bottleneck where polaritons assemble, is located closer to the normal direction compared with the one presented in Figure 3c (i.e., Δ_{TM} = −126.3 meV, P = 400 nm) due to the larger exciton fraction and longer polariton lifetime at smaller detuning energy.[47] When V_{ds} is reduced to −40 V, the emission zone shifts toward the source electrode, resulting in a gradient EL intensity distribution along the *x*-axis (inset of Figure 4b). In this asymmetric electrical injection configuration, the majority of polaritons is driven to propagate along the positive *x* direction (with positive group velocity), as evidenced by the asymmetric EL bands of TM polarization in the experiment (Figure 4b) and the extracted group velocity from the dispersion of LPB-1 and LPB-2 (Figure 4c). The simulated angle-resolved emission using a dipole source on one side of the metasurface to mimic the asymmetric EL distribution shows good correspondence with the experimental results (Figure S7). Specifically, for the polaritonic emission at 1.57 eV, exciton−polaritons are emitted at both 4° and −4° under symmetric injection (V_{ds} = 80 V), while they can be electrically switched to 4° off the normal (with positive group velocity) by changing the source-drain bias to V_{ds} = −40 V (Figure 4d). A similar phenomenon is also observed for TE-polarized polaritons (Figure S8). This mechanism provides a simple way to electrically tune the directionality of the polaritonic emission, which may find applications in actively reconfigurable polaritonic devices. Furthermore, shifting the emission zone between the source and drain electrodes, which is possible in DC-driven LETs operating in the ambipolar regime,[16,37,46] would allow modulation of the polariton emission from positive to negative angles (i.e., with positive or negative group velocities) or at both angles with adjustable ratio, enabling pluridirectional beam steering and ranging.

In conclusion, we demonstrated directional EL from exciton−polaritons in nanostructured $MAPbI_3$ perovskite LETs with a maximum Rabi splitting energy of 206 meV at 78 K. Low damping rates of the photonic BICs supported by the metasurface facilitate their strong coupling with the perovskite excitonic resonance to form polariton BICs under optical or electrical injection. This leads to more than a 50-fold enhancement of EL from the LPB over the excitonic emission of the unpatterned $MAPbI_3$ film. Moreover, the directionality of the polaritonic emission can be reversibly tuned by controlling the carrier distribution within the LET channel with different source-drain biases.

Our proof-of-concept demonstration shows that the light-emitting metatransistor platform, where top-electrode architecture and controllable lateral current injection are compatible with various monolithic cavity designs and metasurface fabrication, enables a complete polaritonic mode and dispersion engineering for the study of strong light−matter interactions under electrical excitation. To assess whether the threshold for polariton lasing is within reach in these systems, we estimated that the charge carrier density in the unoptimized $MAPbI_3$ LET device (1.2×10^{17} cm^{-3}) is only 1 order of magnitude lower than the threshold density obtained for photonic BIC lasing in $MAPbI_3$ metasurfaces (1.6×10^{18} cm^{-3}),[48] which may be even lower for polariton lasing (refer to "Charge carrier density estimation" section in Supporting

https://doi.org/10.1021/acs.nanolett.3c00727
Nano Lett. 2023, 23, 4431−4438

Information). Polariton condensation in perovskite LETs could therefore be achieved employing metasurfaces with improved cavity design to enhance the coupling strength, materials with better optoelectronic properties (e.g., halogen-substituted or 2D perovskites with higher EL yield), and device architectures for higher current injection (e.g., optimized electrode design for intense pulsed bias operation), thus opening new routes toward the highly sought, solution-processed electrically driven laser.[49,50]

■ ASSOCIATED CONTENT

Data Availability Statement

The data that support the findings of this study are openly available in the NTU research data repository DR-NTU (Data) at https://doi.org/10.21979/N9/866ZPH.

Supporting Information

The Supporting Information is available free of charge at https://pubs.acs.org/doi/10.1021/acs.nanolett.3c00727.

Additional text and figures on materials and devices (material synthesis, refractive index dispersion, film thickness determination and device fabrication process workflow), electrical and optical characterization (angle-resolved measurements, schematic of the back focal plane imaging setup, tunable polaritonic EL for TE polarization), numerical simulations (eigenmodes, far field profile), and data analysis (coupled oscillator model, spectral analysis of the polaritonic BIC, strong coupling of the TE_2 and TM_2 bands, charge carrier density estimation) (PDF)

■ AUTHOR INFORMATION

Corresponding Authors

Son Tung Ha − *Institute of Materials Research and Engineering, Agency for Science Technology and Research (A*STAR), Singapore 138634;* orcid.org/0000-0002-5475-8365; Email: Ha_Son_Tung@imre.a-star.edu.sg

Cesare Soci − *Centre for Disruptive Photonic Technologies, TPI and Division of Physics and Applied Physics, School of Physical and Mathematical Sciences, Nanyang Technological University, Singapore 637371;* orcid.org/0000-0002-0149-9128; Email: csoci@ntu.edu.sg

Authors

Yutao Wang − *Centre for Disruptive Photonic Technologies, TPI and Division of Physics and Applied Physics, School of Physical and Mathematical Sciences, Nanyang Technological University, Singapore 637371; Interdisciplinary Graduate School, Energy Research Institute @NTU (ERI@N), Nanyang Technological University, Singapore 637553*

Jingyi Tian − *Centre for Disruptive Photonic Technologies, TPI and Division of Physics and Applied Physics, School of Physical and Mathematical Sciences, Nanyang Technological University, Singapore 637371;* orcid.org/0000-0002-7065-0987

Maciej Klein − *Centre for Disruptive Photonic Technologies, TPI and Division of Physics and Applied Physics, School of Physical and Mathematical Sciences, Nanyang Technological University, Singapore 637371;* orcid.org/0000-0002-3146-4372

Giorgio Adamo − *Centre for Disruptive Photonic Technologies, TPI and Division of Physics and Applied Physics, School of Physical and Mathematical Sciences, Nanyang Technological University, Singapore 637371;* orcid.org/0000-0003-1974-3368

Complete contact information is available at: https://pubs.acs.org/10.1021/acs.nanolett.3c00727

Author Contributions

Y.W. and J.T. contributed equally to this work. C.S., S.T.H., and Y.W. conceived the idea. Y.W. and M.K. fabricated the perovskite LETs. G.A. carried out FIB lithography for metasurface fabrication. Y.W. characterized PL, EL and absorption of the devices with M.K., conducted numerical simulations of the metasurface response and theoretical analysis with J.T. S.T.H. carried out angle-resolved reflection, PL and EL measurements with assistance from Y.W. and M.K. Y.W, J.T., S.T.H. and C.S. performed data analysis and wrote the paper with inputs from all authors.

Notes

The authors declare no competing financial interest.

■ ACKNOWLEDGMENTS

We thank Ramón Paniagua-Domínguez and Arseniy I. Kuznetsov for valuable discussions and advice on this work. Research was supported by the Agency for Science, Technology and Research (A*STAR-AME programmatic grant on Nanoantenna Spatial Light Modulators for Next-Gen Display Technologies, grant no. A18A7b0058) and the Singapore Ministry of Education (grant no. MOE2016-T3-1-006). S.T.H. acknowledges support from AME Young Individual Research Grant (YIRG grant no. A2084c0177) and A*STAR MTC-Programmatic Fund (grant no. M21J9b0085).

■ REFERENCES

(1) Byrnes, T.; Kim, N. Y.; Yamamoto, Y. Exciton−polariton condensates. *Nat. Phys.* **2014**, *10*, 803−813.

(2) Deng, H.; Haug, H.; Yamamoto, Y. Exciton-polariton Bose−Einstein condensation. *Rev. Mod. Phys.* **2010**, *82*, 1489−1537.

(3) Kasprzak, J.; Richard, M.; Kundermann, S.; Baas, A.; Jeambrun, P.; Keeling, J. M. J.; Marchetti, F. M.; Szymanska, M. H.; Andre, R.; Staehli, J. L.; Savona, V.; Littlewood, P. B.; Deveaud, B.; Dang, L. S. Bose−Einstein condensation of exciton polaritons. *Nature* **2006**, *443*, 409−414.

(4) Amo, A.; Lefrère, J.; Pigeon, S.; Adrados, C.; Ciuti, C.; Carusotto, I.; Houdré, R.; Giacobino, E.; Bramati, A. Superfluidity of polaritons in semiconductor microcavities. *Nat. Phys.* **2009**, *5*, 805−810.

(5) Ballarini, D.; De Giorgi, M.; Cancellieri, E.; Houdre, R.; Giacobino, E.; Cingolani, R.; Bramati, A.; Gigli, G.; Sanvitto, D. All-optical polariton transistor. *Nat. Commun.* **2013**, *4*, 1778.

(6) Ballarini, D.; Gianfrate, A.; Panico, R.; Opala, A.; Ghosh, S.; Dominici, L.; Ardizzone, V.; De Giorgi, M.; Lerario, G.; Gigli, G.; Liew, T. C. H.; Matuszewski, M.; Sanvitto, D. Polaritonic Neuromorphic Computing Outperforms Linear Classifiers. *Nano Lett.* **2020**, *20*, 3506−3512.

(7) Christopoulos, S.; von Hogersthal, G. B.; Grundy, A. J.; Lagoudakis, P. G.; Kavokin, A. V.; Baumberg, J. J.; Christmann, G.; Butte, R.; Feltin, E.; Carlin, J. F.; Grandjean, N. Room-temperature polariton lasing in semiconductor microcavities. *Phys. Rev. Lett.* **2007**, *98*, 126405.

(8) Christmann, G.; Butte, R.; Feltin, E.; Carlin, J.-F.; Grandjean, N. Room temperature polariton lasing in a GaN/AlGaN multiple quantum well microcavity. *Appl. Phys. Lett.* **2008**, *93*, 051102.

(9) Liu, X.; Galfsky, T.; Sun, Z.; Xia, F.; Lin, E.-c.; Lee, Y.-H.; Kéna-Cohen, S.; Menon, V. M. Strong light−matter coupling in two-dimensional atomic crystals. *Nat. Photonics* **2015**, *9*, 30−34.

(10) Zhao, L.; Shang, Q.; Li, M.; Liang, Y.; Li, C.; Zhang, Q. Strong exciton-photon interaction and lasing of two-dimensional transition metal dichalcogenide semiconductors. *Nano Research* **2021**, *14*, 1937−1954.
(11) Kéna-Cohen, S.; Forrest, S. R. Room-temperature polariton lasing in an organic single-crystal microcavity. *Nat. Photonics* **2010**, *4*, 371−375.
(12) Ardizzone, V.; Riminucci, F.; Zanotti, S.; Gianfrate, A.; Efthymiou-Tsironi, M.; Suarez-Forero, D. G.; Todisco, F.; De Giorgi, M.; Trypogeorgos, D.; Gigli, G.; Baldwin, K.; Pfeiffer, L.; Ballarini, D.; Nguyen, H. S.; Gerace, D.; Sanvitto, D. Polariton Bose−Einstein condensate from a bound state in the continuum. *Nature* **2022**, *605*, 447−452.
(13) Schneider, C.; Rahimi-Iman, A.; Kim, N. Y.; Fischer, J.; Savenko, I. G.; Amthor, M.; Lermer, M.; Wolf, A.; Worschech, L.; Kulakovskii, V. D.; Shelykh, I. A.; Kamp, M.; Reitzenstein, S.; Forchel, A.; Yamamoto, Y.; Hofling, S. An electrically pumped polariton laser. *Nature* **2013**, *497*, 348−352.
(14) Christogiannis, N.; Somaschi, N.; Michetti, P.; Coles, D. M.; Savvidis, P. G.; Lagoudakis, P. G.; Lidzey, D. G. Characterizing the Electroluminescence Emission from a Strongly Coupled Organic Semiconductor Microcavity LED. *Advanced Optical Materials* **2013**, *1*, 503−509.
(15) Wang, T.; Zang, Z.; Gao, Y.; Lyu, C.; Gu, P.; Yao, Y.; Peng, K.; Watanabe, K.; Taniguchi, T.; Liu, X.; Gao, Y.; Bao, W.; Ye, Y. Electrically Pumped Polarized Exciton-Polaritons in a Halide Perovskite Microcavity. *Nano Lett.* **2022**, *22*, 5175−5181.
(16) Bisri, S. Z.; Takenobu, T.; Iwasa, Y. The pursuit of electrically-driven organic semiconductor lasers. *Journal of Materials Chemistry C* **2014**, *2*, 2827−2836.
(17) Dong, Q.; Fang, Y.; Shao, Y.; Mulligan, P.; Qiu, J.; Cao, L.; Huang, J. Electron-hole diffusion lengths> 175 μm in solution-grown CH3NH3PbI3 single crystals. *Science* **2015**, *347*, 967−970.
(18) Protesescu, L.; Yakunin, S.; Bodnarchuk, M. I.; Krieg, F.; Caputo, R.; Hendon, C. H.; Yang, R. X.; Walsh, A.; Kovalenko, M. V. Nanocrystals of Cesium Lead Halide Perovskites (CsPbX(3), X = Cl, Br, and I): Novel Optoelectronic Materials Showing Bright Emission with Wide Color Gamut. *Nano Lett.* **2015**, *15*, 3692−3696.
(19) Jiang, Y.; Soufiani, A. M.; Gentle, A.; Huang, F.; Ho-Baillie, A.; Green, M. A. Temperature dependent optical properties of $CH_3NH_3PbI_3$ perovskite by spectroscopic ellipsometry. *Appl. Phys. Lett.* **2016**, *108*, 061905.
(20) Makarov, S.; Furasova, A.; Tiguntseva, E.; Hemmetter, A.; Berestennikov, A.; Pushkarev, A.; Zakhidov, A.; Kivshar, Y. Halide-Perovskite Resonant Nanophotonics. *Advanced Optical Materials* **2019**, *7*, 1800784.
(21) Su, R.; Fieramosca, A.; Zhang, Q.; Nguyen, H. S.; Deleporte, E.; Chen, Z.; Sanvitto, D.; Liew, T. C. H.; Xiong, Q. Perovskite semiconductors for room-temperature exciton-polaritonics. *Nat. Mater.* **2021**, *20*, 1315−1324.
(22) Su, R.; Diederichs, C.; Wang, J.; Liew, T. C. H.; Zhao, J.; Liu, S.; Xu, W.; Chen, Z.; Xiong, Q. Room-Temperature Polariton Lasing in All-Inorganic Perovskite Nanoplatelets. *Nano Lett.* **2017**, *17*, 3982−3988.
(23) Dang, N. H. M.; Gerace, D.; Drouard, E.; Trippe-Allard, G.; Ledee, F.; Mazurczyk, R.; Deleporte, E.; Seassal, C.; Nguyen, H. S. Tailoring Dispersion of Room-Temperature Exciton-Polaritons with Perovskite-Based Subwavelength Metasurfaces. *Nano Lett.* **2020**, *20*, 2113−2119.
(24) Su, R.; Ghosh, S.; Wang, J.; Liu, S.; Diederichs, C.; Liew, T. C. H.; Xiong, Q. Observation of exciton polariton condensation in a perovskite lattice at room temperature. *Nat. Phys.* **2020**, *16*, 301−306.
(25) Polimeno, L.; Lerario, G.; De Giorgi, M.; De Marco, L.; Dominici, L.; Todisco, F.; Coriolano, A.; Ardizzone, V.; Pugliese, M.; Prontera, C. T.; Maiorano, V.; Moliterni, A.; Giannini, C.; Olieric, V.; Gigli, G.; Ballarini, D.; Xiong, Q.; Fieramosca, A.; Solnyshkov, D. D.; Malpuech, G.; Sanvitto, D. Tuning of the Berry curvature in 2D perovskite polaritons. *Nat. Nanotechnol* **2021**, *16*, 1349−1354.
(26) Su, R.; Ghosh, S.; Liew, T. C. H.; Xiong, Q. Optical switching of topological phase in a perovskite polariton lattice. *Science Advances* **2021**, *7*, eabf8049.
(27) Dang, N. H. M.; Zanotti, S.; Drouard, E.; Chevalier, C.; Trippe-Allard, G.; Amara, M.; Deleporte, E.; Ardizzone, V.; Sanvitto, D.; Andreani, L. C.; Seassal, C.; Gerace, D.; Nguyen, H. S. Realization of Polaritonic Topological Charge at Room Temperature Using Polariton Bound state in the Contimuum. *Advanced Optical Materials* **2022**, *10*, 2102386.
(28) Masharin, M. A.; Shahnazaryan, V. A.; Benimetskiy, F. A.; Krizhanovskii, D. N.; Shelykh, I. A.; Iorsh, I. V.; Makarov, S. V.; Samusev, A. K. Polaron-Enhanced Polariton Nonlinearity in Lead Halide Perovskites. *Nano Lett.* **2022**, *22*, 9092−9099.
(29) Soci, C.; Adamo, G.; Cortecchia, D.; Wang, K.; Xiao, S.; Song, Q.; Schall-Giesecke, A. L.; Cegielski, P. J.; Lemme, M. C.; Gerace, D.; Sanvitto, D.; Tian, J.; Tonkaev, P. A.; Makarov, S. V.; Kivshar, Y. S.; Jimenez Gordillo, O. A.; Melloni, A.; Pushkarev, A. P.; D'Amato, M.; Lhuillier, E.; Bramati, A. Roadmap on perovskite nanophotonics. *Optical Materials X* **2023**, *17*, 100214.
(30) Huang, C.; Zhang, C.; Xiao, S.; Wang, Y.; Fan, Y.; Liu, Y.; Zhang, N.; Qu, G.; Ji, H.; Han, J.; Ge, L.; Kivshar, Y.; Song, Q. Ultrafast control of vortex microlasers. *Science* **2020**, *367*, 1018−1021.
(31) Zhang, C.; Xiao, S.; Wang, Y.; Gao, Y.; Fan, Y.; Huang, C.; Zhang, N.; Yang, W.; Song, Q. Lead Halide Perovskite-Based Dynamic Metasurfaces. *Laser & Photonics Reviews* **2019**, *13*, 1900079.
(32) Tiguntseva, E. Y.; Zograf, G. P.; Komissarenko, F. E.; Zuev, D. A.; Zakhidov, A. A.; Makarov, S. V.; Kivshar, Y. S. Light-Emitting Halide Perovskite Nanoantennas. *Nano Lett.* **2018**, *18*, 1185−1190.
(33) Maddalena, F.; Chin, X. Y.; Cortecchia, D.; Bruno, A.; Soci, C. Brightness Enhancement in Pulsed-Operated Perovskite Light-Emitting Transistors. *ACS Appl. Mater. Interfaces* **2018**, *10*, 37316−37325.
(34) Chin, X. Y.; Cortecchia, D.; Yin, J.; Bruno, A.; Soci, C. Lead iodide perovskite light-emitting field-effect transistor. *Nat. Commun.* **2015**, *6*, 7383.
(35) Klein, M.; Wang, Y.; Tian, J.; Ha, S. T.; Paniagua-Domínguez, R.; Kuznetsov, A. I.; Adamo, G.; Soci, C. Polarization-Tunable Perovskite Light-Emitting Metatransistor. *Adv. Mater.* **2023**, *35*, 2207317.
(36) Panzer, F.; Li, C.; Meier, T.; Köhler, A.; Huettner, S. Impact of Structural Dynamics on the Optical Properties of Methylammonium Lead Iodide Perovskites. *Adv. Energy Mater.* **2017**, *7*, 1700286.
(37) Chaudhry, M. U.; Muhieddine, K.; Wawrzinek, R.; Sobus, J.; Tandy, K.; Lo, S. C.; Namdas, E. B. Organic Light-Emitting Transistors: Advances and Perspectives. *Adv. Funct. Mater.* **2020**, *30*, 1905282.
(38) Schötz, K.; Askar, A. M.; Peng, W.; Seeberger, D.; Gujar, T. P.; Thelakkat, M.; Köhler, A.; Huettner, S.; Bakr, O. M.; Shankar, K.; Panzer, F. Double peak emission in lead halide perovskites by self-absorption. *Journal of Materials Chemistry C* **2020**, *8*, 2289−2300.
(39) Pazos-Outon, L. M.; Szumilo, M.; Lamboll, R.; Richter, J. M.; Crespo-Quesada, M.; Abdi-Jalebi, M.; Beeson, H. J.; Vrucinic, M.; Alsari, M.; Snaith, H. J.; Ehrler, B.; Friend, R. H.; Deschler, F. Photon recycling in lead iodide perovskite solar cells. *Science* **2016**, *351*, 1430−1433.
(40) Hsu, C. W.; Zhen, B.; Stone, A. D.; Joannopoulos, J. D.; Soljačić, M. Bound states in the continuum. *Nature Reviews Materials* **2016**, *1*, 16048.
(41) Ha, S. T.; Fu, Y. H.; Emani, N. K.; Pan, Z.; Bakker, R. M.; Paniagua-Dominguez, R.; Kuznetsov, A. I. Directional lasing in resonant semiconductor nanoantenna arrays. *Nat. Nanotechnol* **2018**, *13*, 1042−1047.
(42) Guillet, T.; Brimont, C. Polariton condensates at room temperature. *Comptes Rendus Physique* **2016**, *17*, 946−956.
(43) Graf, A.; Held, M.; Zakharko, Y.; Tropf, L.; Gather, M. C.; Zaumseil, J. Electrical pumping and tuning of exciton-polaritons in carbon nanotube microcavities. *Nat. Mater.* **2017**, *16*, 911−917.
(44) Wang, J.; Su, R.; Xing, J.; Bao, D.; Diederichs, C.; Liu, S.; Liew, T. C. H.; Chen, Z.; Xiong, Q. Room Temperature Coherently

https://doi.org/10.1021/acs.nanolett.3c00727
Nano Lett. 2023, 23, 4431−4438

Coupled Exciton-Polaritons in Two-Dimensional Organic-Inorganic Perovskite. *ACS Nano* **2018**, *12*, 8382−8389.
(45) Ballarini, D.; De Giorgi, M.; Gambino, S.; Lerario, G.; Mazzeo, M.; Genco, A.; Accorsi, G.; Giansante, C.; Colella, S.; D'Agostino, S.; Cazzato, P.; Sanvitto, D.; Gigli, G. Polariton-Induced Enhanced Emission from an Organic Dye under the Strong Coupling Regime. *Advanced Optical Materials* **2014**, *2*, 1076−1081.
(46) Klein, M.; Li, J.; Bruno, A.; Soci, C. Co-Evaporated Perovskite Light-Emitting Transistor Operating at Room Temperature. *Advanced Electronic Materials* **2021**, *7*, 2100403.
(47) Gu, J.; Chakraborty, B.; Khatoniar, M.; Menon, V. M. A room-temperature polariton light-emitting diode based on monolayer WS2. *Nat. Nanotechnol* **2019**, *14*, 1024−1028.
(48) Tian, J.; Adamo, G.; Liu, H.; Wu, M.; Klein, M.; Deng, J.; Ang, N. S. S.; Paniagua-Dominguez, R.; Liu, H.; Kuznetsov, A. I.; Soci, C. Phase-Change Perovskite Microlaser with Tunable Polarization Vortex. *Adv. Mater.* **2023**, *35*, e2207430.
(49) Veldhuis, S. A.; Boix, P. P.; Yantara, N.; Li, M.; Sum, T. C.; Mathews, N.; Mhaisalkar, S. G. Perovskite Materials for Light-Emitting Diodes and Lasers. *Adv. Mater.* **2016**, *28*, 6804−6834.
(50) Zhang, Q.; Tao, W.; Huang, J.; Xia, R.; Cabanillas-Gonzalez, J. Toward Electrically Pumped Organic Lasers: A Review and Outlook on Material Developments and Resonator Architectures. *Advanced Photonics Research* **2021**, *2*, 2000155.

https://doi.org/10.1021/acs.nanolett.3c00727
Nano Lett. 2023, 23, 4431−4438